NJC

PAPER

Check for updates

Synthesis, characterization, and enhanced photocatalytic properties of NiWO₄ nanobricks

Saad M. AlShehri,* Jahangeer Ahmed,* Abdulaziz M. Alzahrani and Tansir Ahamad

Brick shaped nanoparticles of nickel tungstate (NiWO₄) were synthesized magnificently using the molten salts process at 500 °C. Powder X-ray diffraction (PXRD) and electron microscopy measurements were carried out to investigate the phase purity, crystal structure, and morphology (size and shape) of the NiWO₄ nanobricks (diameters of ∼20 nm). The BET surface area of the NiWO₄ nanobricks was found to be ∼25 m² g⁻¹. The optical properties of the NiWO₄ nanobricks demonstrate a direct band gap of 2.95 eV. Thereupon, the photocatalytic activities of the NiWO₄ nanobricks have been investigated for the degradation of methylene blue (MB) dye in neutral and basic media under solar light irradiation (SLI). The NiWO₄ nanobricks show significant enhancement in the photo-degradation of MB dye solution in alkaline (∼100% in 50 minutes) and neutral media (∼80% in 330 minutes) as compared to bulk NiWO₄ and previous reports of metal tungstate. ESI mass spectrometry was also carried out to confirm the photocatalytic degradation of dye molecules.

1. Introduction

Semiconducting transition metal tungstate (MWO₄; M = Ti, Co, Ni, Cu, *etc.*) nanostructured materials have received significant attention due to their immeasurably wide range of applications including structural,[1,2] optical,[1–3] transport,[3] electrical,[4] magnetic,[4] sensors,[5,6] metal ion batteries,[7] supercapacitors,[8–11] electrocatalysis,[12–14] antimicrobial,[15] and photocatalysis[15–19]. Titanium dioxides[20–25] or their composites with carbon[26–28] are the most widely used semiconducting photocatalysts. However, in the current decade, nanocrystalline MWO₄ (*e.g.* M = Cu, Co, Ni) particles have been introduced as highly active, efficient, and economical catalysts in photoelectrochemical reactions.[10–17] These metal tungstate nanoparticles exhibit a direct band gap energy in the range from 2.41 eV to 2.95 eV.[19] The low cost, low corrosion, high stability, high activity, and appropriate band gap energy (2.91 eV) of NiWO₄ nanoparticles make them ideal photocatalysts for waste water treatment through the degradation of organic pollutants like methylene blue (MB), Rhodamine B, and methyl orange dyes. Tungsten oxides (WO₃) are also reported as good catalysts in photo-oxidation reactions.[29] The degradation of methylene blue dye solution over the surface of NWO₄ photo-catalysts (N = Ni, Co, Cu, and Zn) was reported previously in the range of degradation from 30–90% for a long irradiation time.[19,30] Liang *et al.* have reported the pH dependent photocatalytic properties of potassium niobate for hydrogen evolution from a water–methanol system.[31] The current work demonstrates the

high photocatalytic performance of NiWO₄ nanobricks for the degradation of organic pollutants in various aqueous media.

Photocatalysis is a simple, eco-friendly, cost effective, and widely accepted process for the eradication of hazardous substances from water. Previously NiWO₄ nanoparticles have been used as the photocatalysts in removal of methylene blue (MB) and methyl orange (MO) dyes from aqueous media,[19,30] but the current work emphasizes the significant enhancement of the photocatalytic activities of NiWO₄ nanoparticles in the degradation of organic dyes (*e.g.* MB) in water at various pH values under solar light irradiation (SLI). MB is a basic dye (aniline dye: C₁₆H₁₈ClN₃S), which causes several health problems like disorders of the central nervous system (CNS), breast cancer, and gastro-intestinal disturbances in human beings.[32–34]

NiWO₄ nanoparticles were prepared from various routes including hydrothermal,[6,35,36] co-precipitation,[16,18,19,37] polyol,[38] and sonochemical[39] methods. Previously, Zuwei Song *et al.* have reported the preparation of NiWO₄ nanoparticles using molten salts (LiNO₃ + NaNO₃), with the precursor materials in the range of molar ratios from 3:1 to 12:1 *via* a ball milling process.[40] Earlier, Ahmed and Mao employed the molten salt process to optimize the formation of 1D oxide nanostructured materials.[41] It is notable that the molten salts procedure is one of the most favorable, simple, eco-friendly, and least expensive procedures to synthesize nanostructured materials. Herein, we report the synthesis of NiWO₄ nanobricks (diameter of ∼20 nm) with a relatively high surface area (∼25 m² g⁻¹) using the modified molten salts (NaNO₃ + KNO₃) process without ball milling. An excess of molten salts works as a solvent like water and plays a significant role in terms of transferring sufficient energy to the

Department of Chemistry, College of Sciences, King Saud University, Riyadh 11451, Kingdom of Saudi Arabia. E-mail: alshehri@ksu.edu.sa, jahmed@ksu.edu.sa

precursor materials to control the shape and size of the final products on the nanometer scale. The single phase crystal structure systems and morphological characterizations were investigated using powder X-ray diffraction (PXRD) and electron microscopy (FESEM and HRTEM) studies, respectively. The optical properties of the $NiWO_4$ nanobricks were studied using a UV-visible spectrophotometer. The photocatalytic applications of the $NiWO_4$ nanobricks for the degradation of MB dye in aqueous media (*i.e.* neutral and alkaline media) were also examined in detail under SLI using a UV-visible spectrophotometer and ESI MS spectrometer.

2. Materials and methods

Two moles of precursor salts of nickel [$Ni(NO_3)_2$; (BDH, 98%)] and tungsten [$Na_2WO_4\cdot 2H_2O$; (BDH, 96%)] with sixty moles of molten salts of sodium nitrate ($NaNO_3$; Alfa Aesar, 98%) and potassium nitrate (KNO_3; Alfa Aesar, 99%) were used in the preparation of $NiWO_4$ nanostructured materials. The precursor and molten salts were ground together for 30 minutes in an agate mortar and pestle and then transferred to a covered crucible. The temperature and time of the reaction were 500 °C and 6 h, respectively. The reaction temperature used was selected according to the reported phase diagram of $NaNO_3$ and KNO_3.[42] The yellow-green colored nanopowders were collected, and this was followed by washing with de-ionized water (four times) and then drying in an oven at 50 °C. The yellowish-green colored powder sample was characterized using a powder X-ray diffractometer (PXRD) containing Ni-filtered Cu-Kα radiation (Rigaku MiniFlex) and FTIR (Bruker TENSOR 27 Spectrometer). FTIR data were recorded at wavenumbers ranging from 400 to 4000 cm^{-1}. FESEM (Field emission scanning electron microscope, JEOL JSM-7600F) and HRTEM (high resolution transmission electron microscope, JEOL JSM-2100F) studies were carried out at 10 and 200 kV, respectively, for morphological characterization. The BET specific surface area of the $NiWO_4$ nanobricks was estimated with a V-Sorb 2800 Porosimetry machine (Gold APP Instruments, China). The optical and photocatalytic properties of the $NiWO_4$ nanoparticles were studied on a UV-vis spectrophotometer (SHIMADZU, UV-1650). The photocatalytic performances of the $NiWO_4$ NBs were examined using aqueous MB dye under solar light irradiation (SLI). The photo-degradation studies of the MB dye solutions were investigated at pH 7 (neutral medium) and 10 (alkaline medium) at room temperature at the λ_{max} of 662.5 nm. The sample solutions with the maximum transparency were taken in a cuvette to examine the photocatalytic degradation of MB dye. The reproducibility of the photocatalytic results was found to be consistent. The rate constant of the photo-degradation (RCP) of MB was calculated using the first-order reaction kinetics [*i.e.* $(\ln(C/C_0) = -kt)$]. An agilent triple quadrupole electro-spray ionization mass spectrometer (ESI MS) was used for the quantitative analysis of the photo-degradation of MB dye.

3. Results and discussions

PXRD studies of the $NiWO_4$ nanobricks show the formation of well crystalline single phase materials with zero impurities (Fig. 1a).
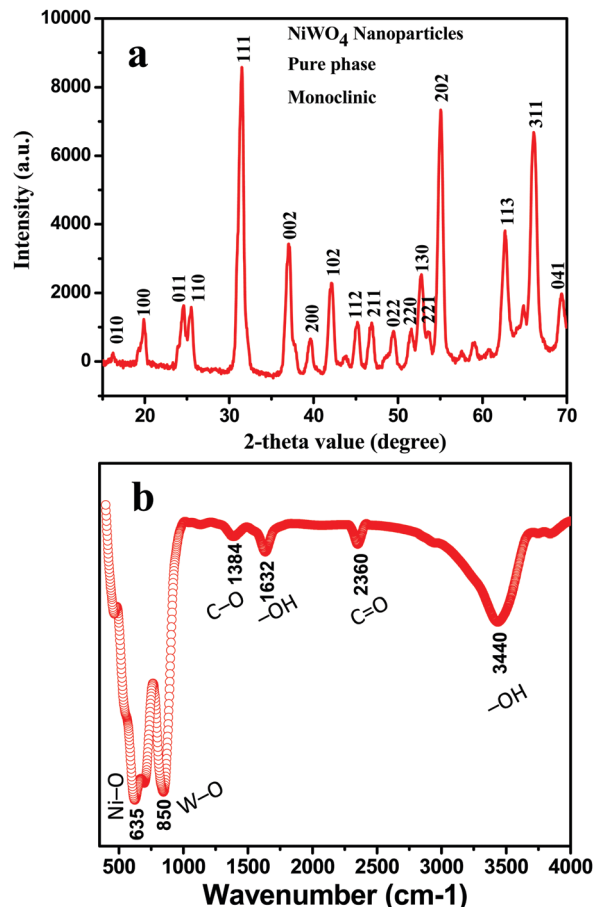

Fig. 1 (a) PXRD and (b) FTIR patterns of the $NiWO_4$ nanobricks.

The diffraction peaks of the $NiWO_4$ nanobricks are indexed to the monoclinic unit cell of $NiWO_4$ (JCPDS # 15-0755). Fig. 1b shows the FTIR spectrum of the $NiWO_4$ nanobricks. The IR bands at wavenumbers of ~ 1384 and ~ 2360 cm^{-1} correspond to the C–O and C=O groups of atmospheric carbon dioxide. The FTIR bands at ~ 1632 and ~ 3440 cm^{-1} correspond to the presence of the O–H group of water. The strong bands at ~ 824 and ~ 635 cm^{-1} agree with the antisymmetric stretching vibration of W–O in $[WO_4]^{2-}$[43] and the Ni–O bonds, which also confirms the establishment of $NiWO_4$.

The FESEM study of $NiWO_4$ shows the formation of particles on the nanometer scale (Fig. 2a). TEM and HRTEM studies were used to further investigate the precise particle size and shape of the nanomaterials. The TEM image of the $NiWO_4$ nanoparticles shows that the nanoparticles are brick shaped with a diameter of ~ 20 nm (Fig. 2b). The high magnification TEM image shows that the brick shaped particles are made up of very small nanoparticles (Fig. 2c). The mean size of these small nanoparticles was observed to be ~ 1 nm. The HRTEM micrograph of the $NiWO_4$ nanobricks demonstrates the formation of lattice fringes on an atomic scale (Fig. 2d). The d-spacing of the lattice fringes of the $NiWO_4$ nanobricks was found to be ~ 2.8 Å from HRTEM, which is in good agreement with the plane ⟨111⟩ of the monoclinic crystal structure of $NiWO_4$, as also supported by the X-ray diffraction patterns.
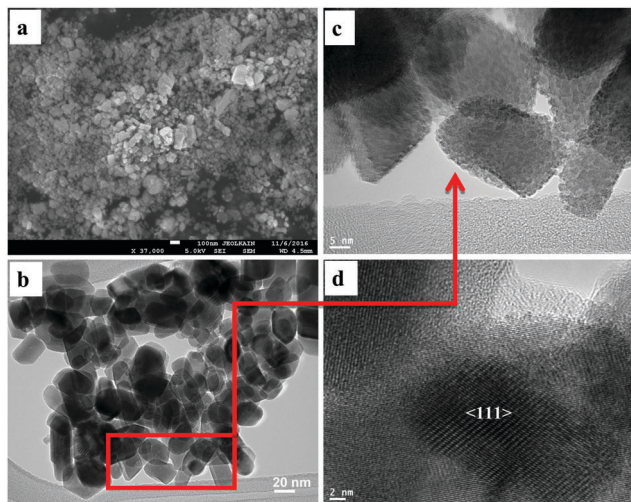
Fig. 2 (a) FESEM, (b) TEM, and (c and d) HRTEM micrographs of the NiWO$_4$ nanobricks.

Fig. 3 (a) EDS analysis and (b) nitrogen adsorption–desorption isotherm of the NiWO$_4$ nanobricks.

Elemental analysis of the nanoparticles was carried out using energy dispersive spectroscopy (EDS) on a FESEM. Energy dispersive studies of the NiWO$_4$ nanobricks confirmed that the elemental compositions of the nanoparticles was in accordance with the initial loaded composition (Fig. 3a). Fig. 3b shows the nitrogen adsorption–desorption isotherm of relative pressure (P/P^0) *vs.* adsorbed volume of nitrogen, to investigate the BET specific surface area of the NiWO$_4$ nanobricks. The specific surface area of NiWO$_4$ nanobricks was found to be $\sim$25 m^2 g^{-1}, which is significantly greater than the previously reported BET surface area of NiWO$_4$ nanoparticles. Previously, the surface area of NiWO$_4$ nanoparticles was reported to be in the range from 2 to 20 m^2 g^{-1}.[16,18,44] The high surface area and quantum size effect of the NiWO$_4$ nanobricks could be significant for the enhanced photocatalytic activity.

The optical properties of the NiWO$_4$ nanobricks were investigated using UV-vis absorption spectroscopic studies at 25 $^\circ$C. The optical absorbance spectrum of the NiWO$_4$ nanobricks was collected and a peak was observed at $\sim$345 nm in the ultraviolet A region (Fig. 4a). The optical band gap energy (*i.e.* direct band gap) of the NiWO$_4$ nanobricks has been estimated using the UV-vis absorption data, following Tauc's model.[45] A plot of photon energy (*i.e.* band gap energy) *vs.* $(\alpha h\nu)^2$ of the NiWO$_4$ nanobricks is shown in Fig. 4b; where α, h and ν are denoted as the absorbance, Planck's constant, and the frequency of the incident beam, respectively. The direct band gap of the NiWO$_4$ nanobricks was found to be $\sim$2.95 eV which closely matches that found in the previous report.[19] The band gap energy is the energy difference between the valence and conduction bands of the material. The NiWO$_4$ nanobricks preserve an appropriate band gap energy in a suitable region to be advantageous for a variety of applications.

The photocatalytic activity of the NiWO$_4$ nanobricks was inspected for the degradation of MB dye under SLI in neutral (pH = 7) and alkaline (pH = 10) media. The photo-degradation of aqueous MB dye to inorganic constituents (*i.e.* H$_2$O, CO$_2$, *etc.*)
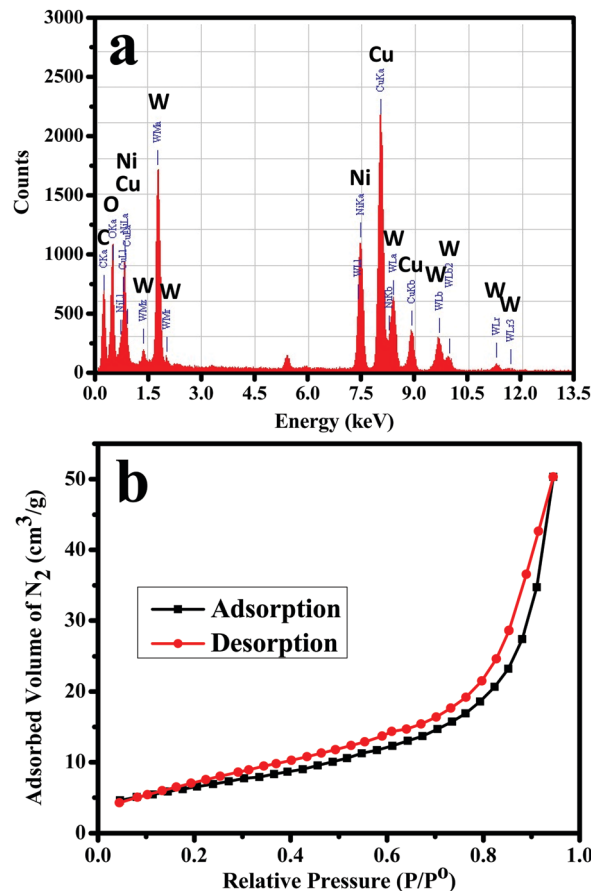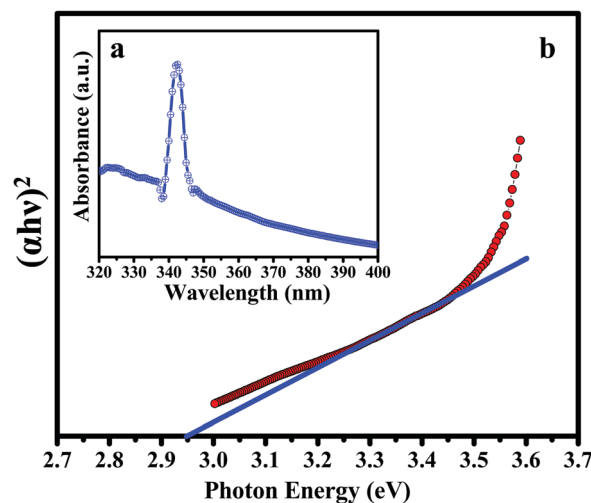

Fig. 4 (a) UV-visible absorption spectrum and (b) band gap energy plot [$(\alpha h\nu)^2$ *vs.* photon energy (eV)] of the NiWO$_4$ nanobricks.

over the surface of the NiWO$_4$ nanobricks can be described by the generation of hydroxyl free radicals (OH$^\bullet$), as shown in Fig. 5a. The photocatalytic performance of the NiWO$_4$ nanobricks could happen due to the electron (e$^-$)–hole (h$^+$) pairs.
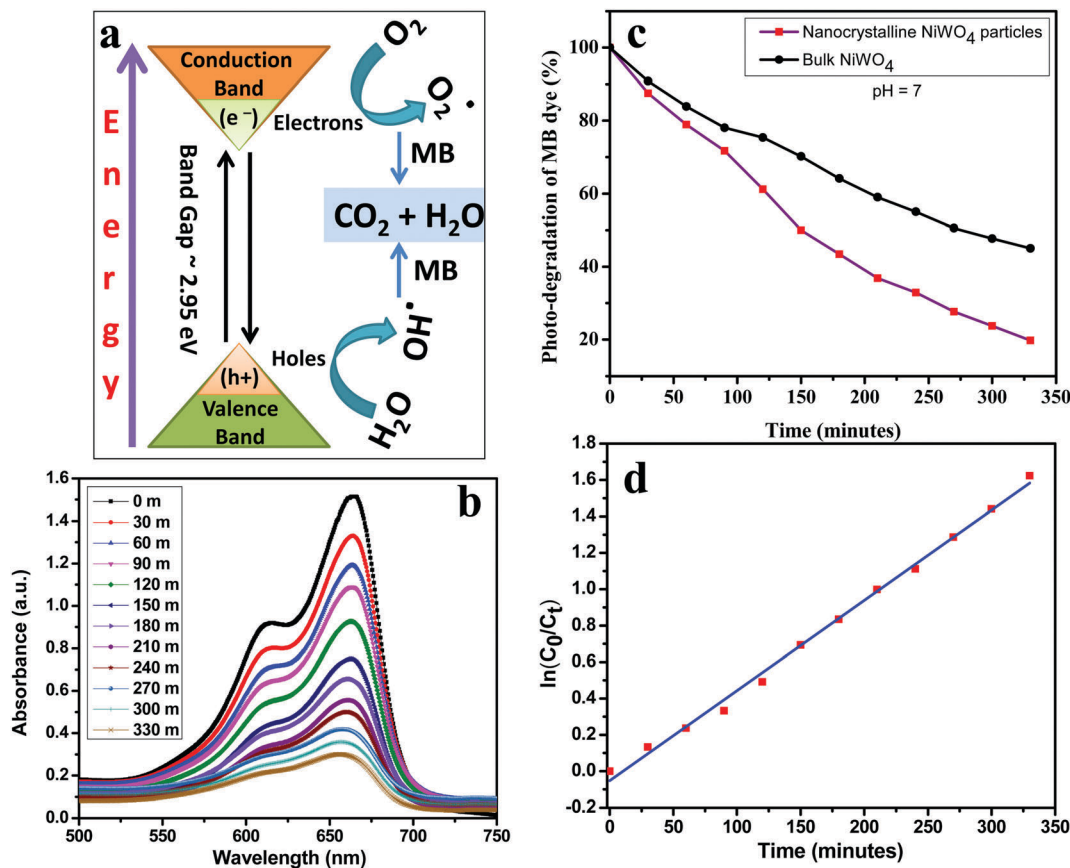
Fig. 5 The (a) mechanism, (b) absorption spectra, (c) percentage degradation of MB with the NiWO$_4$ nanobricks and bulk NiWO$_4$, and (d) linear plots of the photo-degradation of MB with the NiWO$_4$ nanobricks under SLI at pH 7.

The e$^-$ and h$^+$ pairs may produce a super-oxide radical anion (*i.e.* O$_2$$^{-\bullet}$) and hydroxyl radicals (*i.e.* OH$^\bullet$), respectively, in an aqueous medium. The OH$^\bullet$ attacks the MB dye molecules to oxidize it into its inorganic constituents (*e.g.* H$_2$O, CO$_2$, NO$_3$$^-$, *etc.*).

The photo-degradation of aqueous MB dye over the surface of the NiWO$_4$ nanobricks under SLI was investigated at pH 7 using the UV-vis absorption spectra at the maximum absorbance value of 663.5 nm for 330 minutes (Fig. 5b). The absorption band intensities of the MB dye solution were reduced with time (t) under SLI, indicating the degradation of MB dye on the surface of the NiWO$_4$ nanobricks. Fig. 5c shows the percentage photo-degradation of the MB dye solution with time (t). Photocatalytic degradation performances were calculated using the following equation: (C_t/C_0) $\times$ 100%, where, C_t and C_0 are the concentration after time 't' and time '0'. The NiWO$_4$ nanobricks degrade >80% of the MB dye when under SLI for 330 minutes, while no degradation of the MB dye was observed in the dark with catalysts present. Moreover, no photo-degradation occurred in the presence of solar light without catalysts. The photocatalytic degradation reactions of the MB dye using bulk NiWO$_4$ particles have also been investigated. We observed that the photocatalytic activity of the NiWO$_4$ NBs is found to be much higher than that of the bulk NiWO$_4$ particles at pH 7 (Fig. 5c). The stability of the photocatalysts was also studied *via* recycling processes. These photocatalysts have significant recycled

efficiencies, with good activity for the degradation of aqueous MB dye under SLI. It is noteworthy that the NiWO$_4$ photocatalysts retain up to ~60% of their photocatalytic performances for 330 minutes after five sequential cycles under SLI at pH 7. Fig. 5d shows the linear plot of ln(C_0/C_t) *versus* time for the photo-degradation of MB dye with the NiWO$_4$ photocatalysts, in order to study the kinetics of the photochemical reactions. The rate constant of the photochemical reactions was estimated from the linear slope fitting curve. The photochemical reactions follow first-order decay kinetics. The value of the rate constant (k) and R^2 were found to be 0.00496 minute^{-1} and 0.9955, respectively (Table 1).

Moreover, the photocatalytic degradation of MB dye was also explored in a basic medium (*i.e.* pH = 10) using the NiWO$_4$ photocatalysts under SLI. Fig. 6a shows the absorption spectra of aqueous MB dye at 662.5 nm (maximum wavelength) with photocatalysts. The photocatalytic degradation reaction of MB

Table 1 Resulting kinetic parameters of the photocatalytic degradation of MB dye obtained in neutral and alkaline media

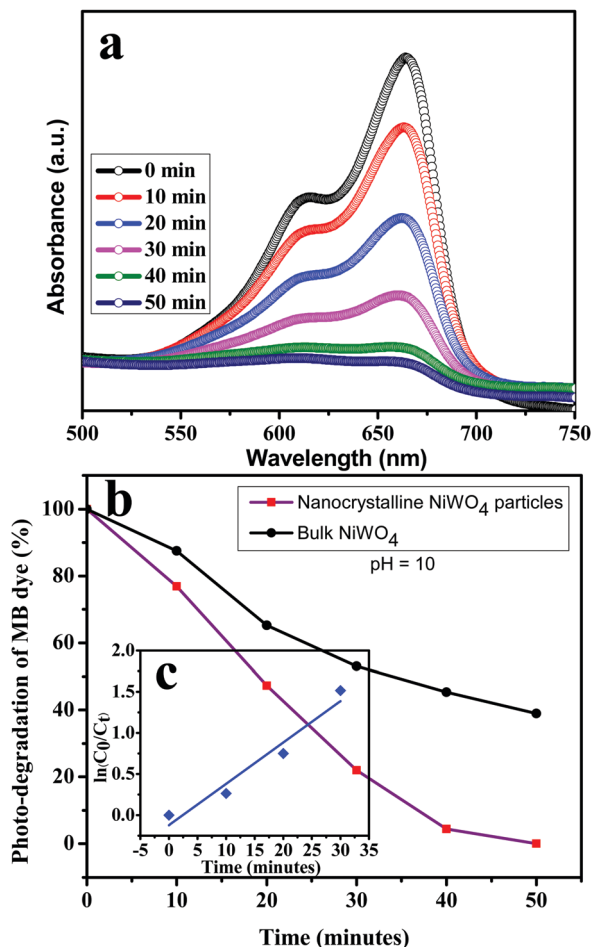| Medium	pH	Photo-degradation of MB dye	k (min^{-1})	R^2	Decay kinetics
Neutral	7	80% within 330 minutes	0.00496	0.9955	First-order
Alkaline	10	100% within 50 minutes	0.0503	0.9289	First-order

Fig. 6 The (a) absorption spectra, (b) percentage degradation of MB with the NiWO$_4$ nanobricks and bulk NiWO$_4$, and (c) linear plot of photo-catalytic degradation of MB dye under SLI at pH 10.

Fig. 7 Histogram showing the regeneration efficiency of the NiWO$_4$ photocatalysts at pH values of 7 and 10.

dye is faster in the basic medium than in the neutral medium. The photo-degradation of MB dye was completed in only 50 minutes at a pH value of 10, which is found to be ∼7 times faster than that for the neutral medium (pH = 7). Photocatalytic activities of the NiWO$_4$ nanobricks in the basic medium (pH = 10) are shown in Fig. 6b. The photo-degradation reaction of MB dye was ∼93% complete within 40 minutes and 100% within 50 minutes under SLI. The rate of the photocatalytic degradation of organic pollutants depends on the surface area of the material and the nature of the medium. A larger number of hydroxyl radicals (oxidizing agents) could be formed in an alkaline medium compared to a neutral medium, and the rate of photochemical reactions would be higher. The NiWO$_4$ nanobricks show a significant enhancement in the photocatalytic degradation of MB compared to that of bulk NiWO$_4$ particles in an alkaline medium, as is also shown in Fig. 6b. The photo-degradation of MB dye over the surface of the NiWO$_4$ photocatalysts was reported previously in the range of degradation from 30–90% for a longer irradiation period (400 minutes).[30] Previously, the photocatalytic degradation capacities of metal tungstate nanoparticles have also been evaluated for the de-colorization of organic dyes under SLI. The photocatalytic degradation of
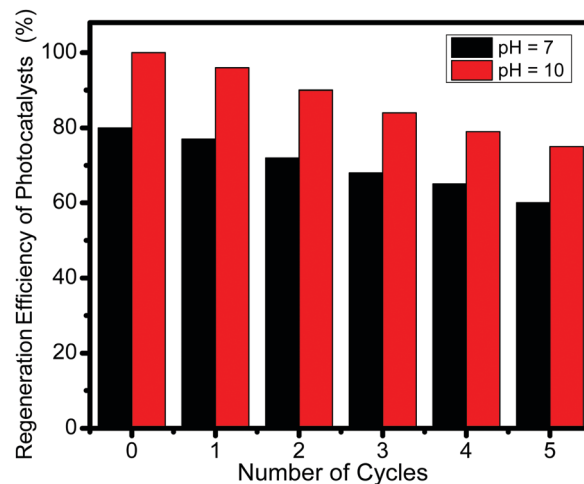
MB dye with CoWO$_4$, CuWO$_4$, and ZnWO$_4$ photocatalysts was reported to be 30%, 70%, and 90%, respectively, within 120 minutes, while MO dye was de-colorized only up to 20%
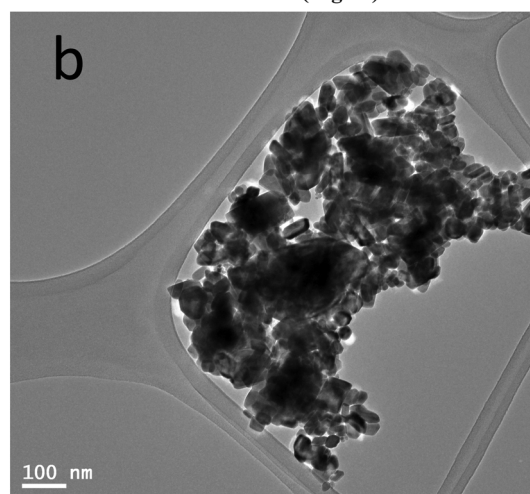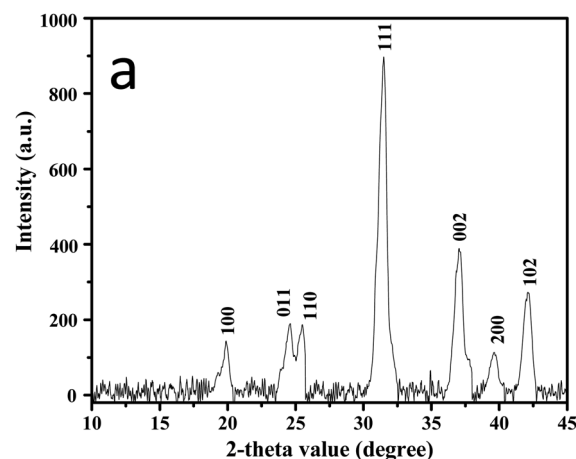

Fig. 8 The (a) XRD pattern and (b) TEM image of the NiWO$_4$ nanobricks after photo-degradation of MB dye.
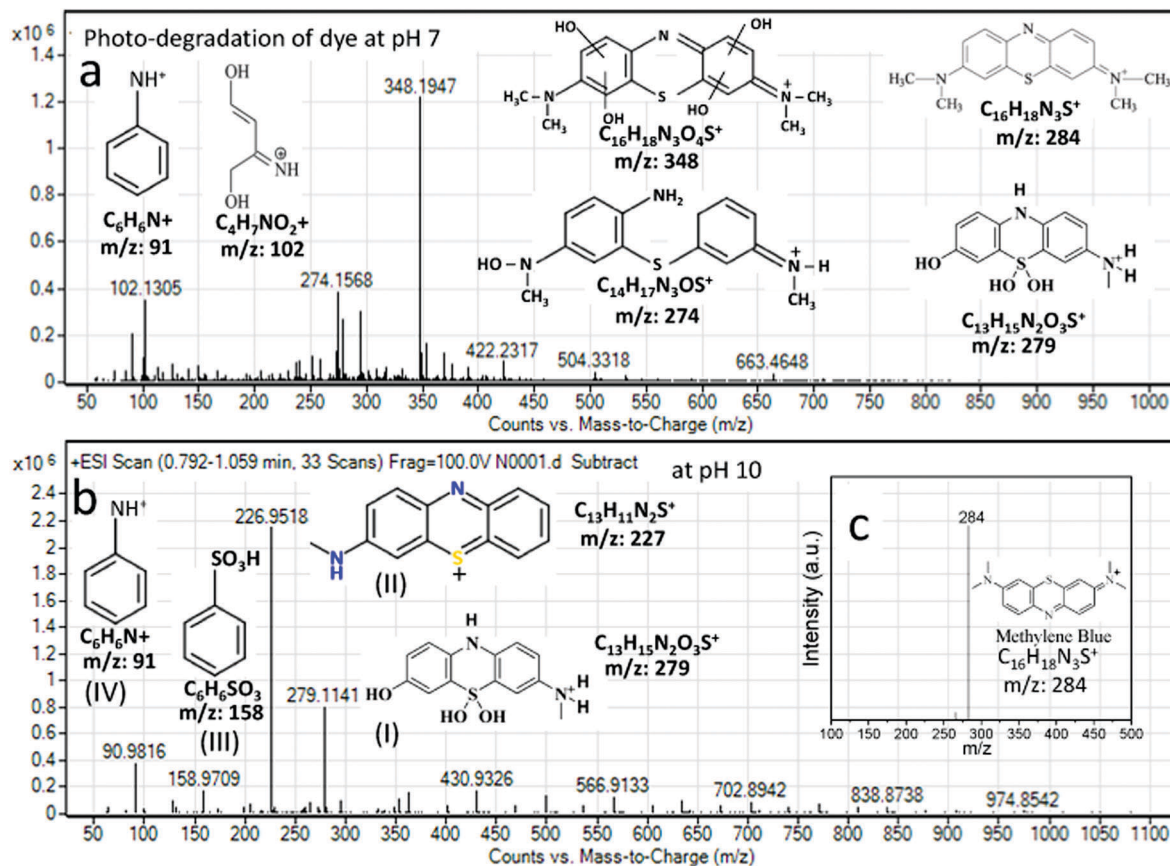
Fig. 9 ESI mass spectrometric spectra of MB dye solution (a) after photocatalytic degradation at pH 7, (b) after photocatalytic degradation at pH 10, and (c) without photocatalytic degradation *i.e.* pure MB dye.

in 120 minutes over the surface of MWO4 (M = Ni, Co, and Cu).[19] Barium tungstate (BaWO$_4$) nanoparticles were reported for the degradation of methyl orange and Rhodamine B dyes with percentages of ~70% after 70 minutes and ~90% after 180 minutes under SLI.[43,46] Recently, the photocatalytic degradation of MB dye with WO$_3$ nanoparticles was reported to be ~20% in 160 minutes.[47] Therefore, the present work demonstrates the enhanced photocatalytic activity of the NiWO$_4$ nanobricks in the de-colorization of MB dye solution under SLI. Fig. 6c shows the kinetic linear plot of $\ln(C_0/C_t)$ *vs.* time 't', which follows the pseudo-first order kinetics. The rate constants and R^2 values were found to be 0.0503 min^{-1}, and ~0.9289, respectively, as is also shown in Table 1.

The stability and regeneration efficiencies of the NiWO$_4$ photocatalysts have been investigated over five consecutive cycles at different pH values (7 and 10) under solar light irradiation. The NiWO$_4$ nanobricks are recyclable and efficient photocatalytic materials for the degradation of MB dye. We observed that the NiWO$_4$ nanobricks retain photocatalytic regeneration efficiencies of ~60% and ~80% for up to five consecutive cycles under solar light irradiation at pH values of 7 and 10, respectively (Fig. 7). Note that the photocatalysts were washed appropriately using the deionized water and dried properly at 60 °C prior to performing a new cycle of the experiment. Moreover, we have checked the crystalline nature

and morphology of the NiWO$_4$ nanobricks after photo-degradation of MB using XRD and TEM studies (Fig. 8a and b). We observed that the intensity of the lines decreases and the background increases, but the nature of the material was still crystalline. The TEM study of the materials (obtained after the photo-degradation process) shows some changes in the morphology, like agglomeration of the particles.

ESI mass spectrometric studies were also carried out in neutral (pH = 7) and alkaline (pH = 10) media in order to understand the fragmentation of the MB dye during the photo-degradation process. Fig. 9a shows the ESI-MS data of the MB dye after the photo-degradation at pH 7. The m/z signals at ~358 ($C_{16}H_{18}N_3O_4S^+$), ~279 ($C_{13}H_{15}N_2O_3S^+$), ~274 ($C_{14}H_{17}N_3OS^+$), ~102 ($C_4H_7NO_2^+$), and ~91 ($C_6H_6N^+$) correspond to the fragmented intermediates of the MB dye solution generated by the attack of free radicals. ESI mass spectral studies showed the complete degradation of MB dye molecules after 50 minutes under SLI and no peak was detected at m/z of 284, as shown in Fig. 9b. The signals at m/z = ~279, ~227, ~158, and ~91 could be received on the basis of the fragmented intermediates that confirm the photo-degradation of the dye molecule by the attack of free radicals. C–N and C–S are the most active bonds of the MB dye that could be broken readily by the attack of free radicals (*i.e.* hydroxyl and superoxide) resulting in the oxidized organic molecules (*i.e.* intermediates).

The fragmented intermediates further degrade into inorganic constituents at a long irradiation time. Ammar *et al.* have reported the degradation of MB dye molecules followed by the mineralization of organic carbon into CO_2, and hetero-atoms (*e.g.* S and N *etc.*) into inorganic ions (*e.g.* sulfate, nitrate and ammonium ions *etc.*) or other volatile compounds at a long irradiation period (>1000 minutes).[48] Our results are in good agreement with the previous work reporting on the oxidative degradation of MB dye using metal oxide nanoparticles as the catalysts.[49–51] Fig. 9c shows that the molecular ion peak of MB dye (before degradation) was obtained at an *m/z* value of 284 as also reported previously.[52]

4. Conclusions

Single phase $NiWO_4$ nanobricks have been synthesized using the molten salts process at 500 °C. The optical properties of the $NiWO_4$ nanobricks revealed a direct band gap of ~2.95 eV, from the absorption spectroscopy studies. The $NiWO_4$ photocatalysts significantly degrade a MB dye solution in neutral and alkaline media, compared to bulk $NiWO_4$ or previous reports on metal tungstate. These photocatalysts showed good recyclable efficiencies in both media. ESI-MS spectral studies were employed to study the fragmented molecules obtained by the photodegradation of MB dye. The current work could be industrially significant for waste water treatment on a large scale by the removal of hazardous substances from water under SLI.

Acknowledgements

References

1 S. V. Green, C. G. Granqvist and G. A. Niklasson, Structure and optical properties of electrochromic tungsten-containing nickel oxide films, *Sol. Energy Mater. Sol. Cells*, 2014, **126**, 248–259.

2 T. Siritanon, A. Jiamprasertboon and N. Yong, Structure and optical properties of $Ni_{1-x}Co_xWO_4$ solid solutions, *Mater. Lett.*, 2015, **145**, 316–320.

3 B. Sawicki, T. Groń, E. Tomaszewicz, H. Duda and K. Górny, Some optical and transport properties of a new subclass of ceramic tungstates and molybdates, *Ceram. Int.*, 2015, **41**, 13080–13089.

4 S. Shanmugapriya, S. Surendran, V. D. Nithya, P. Saravanan and R. Kalai Selvan, Temperature dependent electrical and magnetic properties of $CoWO_4$ nanoparticles synthesized by sonochemical method, *Mater. Sci. Eng., B*, 2016, **214**, 57–67.

5 F. Li, Q. Qin, N. Zhang, C. Chen, L. Sun, X. Liu, Y. Chen, C. Li and S. Ruan, Improved gas sensing performance with Pd-doped $WO_3 \cdot H_2O$ nanomaterials for the detection of xylene, *Sens. Actuators, B*, 2017, **244**, 837–848.

6 S. Mani, V. Vediyappan, S.-M. Chen, R. Madhu, V. Pitchaimani, J.-Y. Chang and S.-B. Liu, Hydrothermal synthesis of $NiWO_4$ crystals for high performance non-enzymatic glucose bio-sensors, *Sci. Rep.*, 2016, **6**, 24128.

7 T. Peng, C. Liu, X. Hou, Z. Zhang, C. Wang, H. Yan, Y. Lu, X. Liu and Y. Luo, Control Growth of Mesoporous Nickel Tungstate Nanofiber and Its Application as Anode Material for Lithium-Ion Batteries, *Electrochim. Acta*, 2017, **224**, 460–467.

8 Y. Wang, C. Shen, L. Niu, Z. Sun, F. Ruan, M. Xu, S. Shan, C. Li, X. Liu and Y. Gong, High rate capability of mesoporous $NiWO_4$–$CoWO_4$ nanocomposite as a positive material for hybrid supercapacitor, *Mater. Chem. Phys.*, 2016, **182**, 394–401.

9 Y. He, L. Wang, D. Jia, Z. Zhao and J. Qiu, $NiWO_4$/Ni/Carbon Composite Fibres for Supercapacitors with Excellent Cycling Performance, *Electrochim. Acta*, 2016, **222**, 446–454.

10 X. Xu, L. Pei, Y. Yang, J. Shen and M. Ye, Facile synthesis of $NiWO_4$/reduced graphene oxide nanocomposite with excellent capacitive performance for supercapacitors, *J. Alloys Compd.*, 2016, **654**, 23–31.

11 U. Nithiyanantham, S. R. Ede, S. Anantharaj and S. Kundu, Self-Assembled $NiWO_4$ Nanoparticles into Chain-like Aggregates on DNA Scaffold with Pronounced Catalytic and Super-capacitor Activities, *Cryst. Growth Des.*, 2015, **15**, 673–686.

12 D. Gubán, I. Borbáth, Z. Pászti, I. Sajó, E. Drotár, M. Hegedűs and A. Tompos, Preparation and characterization of novel $Ti_{0.7}W_{0.3}O_2$–C composite materials for Pt-based anode electrocatalysts with enhanced CO tolerance, *Appl. Catal., B*, 2015, **174–175**, 455–470.

13 V. K. V. P. Srirapu, A. Kumar, P. Srivastava, R. N. Singh and A. S. K. Sinha, Nanosized $CoWO_4$ and $NiWO_4$ as efficient oxygen-evolving electrocatalysts, *Electrochim. Acta*, 2016, **209**, 75–84.

14 E. Antolini and E. R. Gonzalez, Tungsten-based materials for fuel cell applications, *Appl. Catal., B*, 2010, **96**, 245–266.

15 R. Karthiga, B. Kavitha, M. Rajarajan and A. Suganthi, Photocatalytic and antimicrobial activity of $NiWO_4$ nano-particles stabilized by the plant extract, *Mater. Sci. Semicond. Process.*, 2015, **40**, 123–129.

16 U. M. García-Pérez, A. Martínez-delaCruz and J. Peral, Transition metal tungstates synthesized by co-precipitation method: Basic photocatalytic properties, *Electrochim. Acta*, 2012, **81**, 227–232.

17 Y. Keereeta, S. Thongtem and T. Thongtem, Enhanced photocatalytic degradation of methylene blue by WO_3/$ZnWO_4$ composites synthesized by a combination of microwave-solvothermal method and incipient wetness procedure, *Powder Technol.*, 2015, **284**, 85–94.

18 X. A. López, A. F. Fuentes, M. M. Zaragoza, J. A. Díaz Guillén, J. S. Gutiérrez, A. L. Ortiz and V. Collins-Martínez, Synthesis, characterization and photocatalytic evaluation of MWO_4 (M = Ni, Co, Cu and Mn) tungstates, *Int. J. Hydrogen Energy*, 2016, **41**, 23312–23317.

19 T. Montini, V. Gombac, A. Hameed, L. Felisari, G. Adami and P. Fornasiero, Synthesis, characterization and photocatalytic

performance of transition metal tungstates, *Chem. Phys. Lett.*, 2010, **498**, 113–119.

20 D. Das, A. Shivhare, S. Saha and A. K. Ganguli, Room temperature synthesis of mesoporous TiO_2 nanostructures with high photocatalytic efficiency, *Mater. Res. Bull.*, 2012, **47**, 3780–3785.

21 M. Qamar, S. J. Kim and A. K. Ganguli, TiO_2-based nanotubes modified with nickel: synthesis, properties, and improved photocatalytic activity, *Nanotechnology*, 2009, **20**, 455703.

22 E. M. Seftel, M. Niarchos, C. Mitropoulos, M. Mertens, E. F. Vansant and P. Cool, Photocatalytic removal of phenol and methylene-blue in aqueous media using TiO_2@LDH clay nanocomposites, *Catal. Today*, 2015, **252**, 120–127.

23 H. Huang, D. Y. C. Leung, P. C. W. Kwong, J. Xiong and L. Zhang, Enhanced photocatalytic degradation of methylene blue under vacuum ultraviolet irradiation, *Catal. Today*, 2013, **201**, 189–194.

24 G. Zhang, S. Zhang, L. Wang, R. Liu, Y. Zeng, X. Xia, Y. Liu and S. Luo, Facile synthesis of bird's nest-like TiO_2 microstructure with exposed (001) facets for photocatalytic degradation of methylene blue, *Appl. Surf. Sci.*, 2017, **391**(Part B), 228–235.

25 B. Liu, A. Khare and E. S. Aydil, TiO_2–B/Anatase Core–Shell Heterojunction Nanowires for Photocatalysis, *ACS Appl. Mater. Interfaces*, 2011, **3**, 4444–4450.

26 Y. Yang, L. Xu, H. Wang, W. Wang and L. Zhang, TiO_2/graphene porous composite and its photocatalytic degradation of methylene blue, *Mater. Des.*, 2016, **108**, 632–639.

27 X. Luan, M. T. Gutierrez Wing and Y. Wang, Enhanced photocatalytic activity of graphene oxide/titania nanosheets composites for methylene blue degradation, *Mater. Sci. Semicond. Process.*, 2015, **30**, 592–598.

28 J. G. Radich, A. L. Krenselewski, J. Zhu and P. V. Kamat, Is Graphene a Stable Platform for Photocatalysis? Mineralization of Reduced Graphene Oxide With UV-Irradiated TiO_2 Nanoparticles, *Chem. Mater.*, 2014, **26**, 4662–4668.

29 N. Zhang, C. Chen, Z. Mei, X. Liu, X. Qu, Y. Li, S. Li, W. Qi, Y. Zhang, J. Ye, V. A. L. Roy and R. Ma, Monoclinic Tungsten Oxide with {100} Facet Orientation and Tuned Electronic Band Structure for Enhanced Photocatalytic Oxidations, *ACS Appl. Mater. Interfaces*, 2016, **8**, 10367–10374.

30 M. M. Mohamed, S. A. Ahmed and K. S. Khairou, Unprecedented high photocatalytic activity of nanocrystalline WO_3/$NiWO_4$ hetero-junction towards dye degradation: effect of template and synthesis conditions, *Appl. Catal., B*, 2014, **150–151**, 63–73.

31 B. Liang, N. Zhang, C. Chen, X. Liu, R. Ma, S. Tong, Z. Mei, V. A. L. Roy, H. Wang and Y. Tang, Hierarchical yolk–shell layered potassium niobate for tuned pH-dependent photocatalytic H_2 evolution, *Catal. Sci. Technol.*, 2017, **7**, 1000–1005.

32 M. D. P. D. L. Vutskits, A. Briner, P. Klauser, M. D. P. D. E. Gascon, M. D. Alexandre, G. Dayer, M. D. Jozsef, Z. Kiss, M. D. P. D. D. Muller, M. D. Marc, J. Licker, M. D. Denis and R. Morel, Adverse Effects of Methylene Blue on the Central Nervous System, *Anesthesiology*, 2008, **108**, 684–692.

33 N. Piscatelli, S. Crawford, A. Larkin, Q. Robert and R. Layeequr Rahman, Complications of methylene blue dye infiltration for sentinel lymph node biopsy in breast cancer, *Cancer Res.*, 2009, **69**, 4140.

34 M. Kida, K. Kobayashi and K. Saigenji, Routine chromo-endoscopy for gastrointestinal diseases: indications revised, *Endoscopy*, 2003, **35**, 590–596.

35 M. I. Ahmed, A. Adam, A. Khan, M. N. Siddiqui, Z. H. Yamani and M. Qamar, Synthesis of mesoporous $NiWO_4$ nanocrystals for enhanced photoelectrochemical water oxidation, *Mater. Lett.*, 2016, **177**, 135–138.

36 Y. Bi, H. Nie, D. Li, S. Zeng, Q. Yang and M. Li, $NiWO_4$ nanoparticles: a promising catalyst for hydrodesulfurization, *Chem. Commun.*, 2010, **46**, 7430–7432.

37 S. M. Pourmortazavi, M. Rahimi-Nasrabadi, M. Khalilian-Shalamzari, M. M. Zahedi, S. S. Hajimirsadeghi and I. Omrani, Synthesis, structure characterization and catalytic activity of nickel tungstate nanoparticles, *Appl. Surf. Sci.*, 2012, **263**, 745–752.

38 J. Ungelenk, M. Speldrich, R. Dronskowski and C. Feldmann, Polyol-mediated low-temperature synthesis of crystalline tungstate nanoparticles MWO_4 (M = Mn, Fe, Co, Ni, Cu, Zn), *Solid State Sci.*, 2014, **31**, 62–69.

39 R. Talebi, Simple sonochemical synthesis and characterization of nickel tungstate nanoparticles and its photocatalyst application, *J. Mater. Sci.: Mater. Electron.*, 2016, **27**, 3565–3569.

40 Z. Song, J. Ma, H. Sun, W. Wang, Y. Sun, L. Sun, Z. Liu and C. Gao, Synthesis of $NiWO_4$ nano-particles in low-temperature molten salt medium, *Ceram. Int.*, 2009, **35**, 2675–2678.

41 J. Ahmed and Y. Mao, Ultrafine Iridium Oxide Nanorods Synthesized by Molten Salt Method toward Electrocatalytic Oxygen and Hydrogen Evolution Reactions, *Electrochim. Acta*, 2016, **212**, 686–693.

42 C. M. Kramer and C. J. Wilson, The phase diagram of $NaNO_3$–KNO_3, *Thermochim. Acta*, 1980, **42**, 253–264.

43 M. Mohamed Jaffer Sadiq and A. Samson Nesaraj, Soft chemical synthesis and characterization of $BaWO_4$ nanoparticles for photocatalytic removal of Rhodamine B present in water sample, *J. Nanostruct. Chem.*, 2015, **5**, 45–54.

44 L. Pan, L. Li and Y. Chen, Synthesis and electrocatalytic properties of microsized Ag_2WO_4 and nanoscaled MWO_4 (M = Co, Mn), *J. Sol-Gel Sci. Technol.*, 2013, **66**, 330–336.

45 J. Tauc, Optical properties and electronic structure of amorphous Ge and Si, *Mater. Res. Bull.*, 1968, **3**, 37–46.

46 S. Khademolhoseini and S. Ali Zarkar, Preparation and characterization of barium tungstate nanoparticles via a new simple surfactant-free route, *J. Mater. Sci.: Mater. Electron.*, 2016, **27**, 9605–9609.

47 B. Ahmed, S. Kumar, A. K. Ojha, P. Donfack and A. Materny, Facile and controlled synthesis of aligned WO_3 nanorods and nanosheets as an efficient photocatalyst material, *Spectrochim. Acta, Part A*, 2017, **175**, 250–261.

48 A. Houas, H. Lachheb, M. Ksibi, E. Elaloui, C. Guillard and J.-M. Herrmann, Photocatalytic degradation pathway of methylene blue in water, *Appl. Catal., B*, 2001, **31**, 145–157.

49 H. S. Oliveira, L. C. A. Oliveira, M. C. Pereira, J. D. Ardisson, P. P. Souza, P. O. Patricio and F. C. C. Moura, Nanostructured vanadium-doped iron oxide: catalytic oxidation of methylene blue dye, *New J. Chem.*, 2015, **39**, 3051–3058.

50 M. Amini, B. Pourbadiei, T. P. A. Ruberu and L. K. Woo, Catalytic activity of MnO_x/WO_3 nanoparticles: synthesis, structure characterization and oxidative degradation of methylene blue, *New J. Chem.*, 2014, **38**, 1250–1255.

51 T. Ahmad, R. Phul, P. Alam, I. H. Lone, M. Shahazad, J. Ahmed, T. Ahamad and S. Alshehri, Dielectric, optical and enhanced photocatalytic properties of $CuCrO_2$ nanoparticles, *RSC Adv.*, 2017, **7**, 27549–27557.

52 A. Molla, M. Sahu and S. Hussain, Under dark and visible light: fast degradation of methylene blue in the presence of Ag–In–Ni–S nanocomposites, *J. Mater. Chem. A*, 2015, **3**, 15616–15625.

This journal is © The Royal Society of Chemistry and the Centre National de la Recherche Scientifique 2017